A new method and a new index for identifying socioeconomic drought events under climate change: a case study of the East River basin in China

Haiyun SHI [a,b], Ji CHEN [a,*], Keyi WANG [c], Jun NIU [d,e]

[a] *Department of Civil Engineering, The University of Hong Kong, Hong Kong, China*

[b] *State Key Laboratory of Plateau Ecology and Agriculture, Qinghai University, Xining, Qinghai, China*

[c] *State Key Laboratory of Hydroscience & Engineering, Tsinghua University, Beijing, China*

[d] *Center for Agricultural Water Research in China, China Agricultural University, Beijing, China*

[e] *College of Water Resources & Civil Engineering, China Agricultural University, Beijing, China*

* Corresponding author (Dr. Ji CHEN): jichen@hku.hk

Revised Manuscript for *Science of the Total Environment*

October 2017

Abstract

Drought is a complex natural hazard that may have destructive damages on societal properties and even lives. Generally, socioeconomic drought occurs when water resources systems cannot meet water demand, mainly due to a weather-related shortfall in water supply. This study aims to propose a new method, a heuristic method, and a new index, the socioeconomic drought index (SEDI), for identifying and evaluating socioeconomic drought events on different severity levels (i.e., slight, moderate, severe, and extreme) in the context of climate change. First, the minimum in-stream water requirement (MWR) is determined through synthetically evaluating the requirements of water quality, ecology, navigation, and water supply. Second, according to the monthly water deficit calculated as the monthly streamflow data minus the MWR, the drought month can be identified. Third, according to the cumulative water deficit calculated from the monthly water deficit, drought duration (i.e., the number of continuous drought months) and water shortage (i.e., the largest cumulative water deficit during the drought period) can be detected. Fourth, the SEDI value of each socioeconomic drought event can be calculated through integrating the impacts of water shortage and drought duration. To evaluate the applicability of the new method and new index, this study examines the drought events in the East River basin in South China, and the impact of a multi-year reservoir (i.e., the Xinfengjiang Reservoir) in this basin on drought analysis is also investigated. The historical and future streamflow of this basin is simulated using a hydrologic model, Variable Infiltration Capacity (VIC) model. For historical and future drought analysis, the proposed new method and index are feasible to identify socioeconomic drought events. The results show that a number of

socioeconomic drought events (including some extreme ones) may occur in future, and the appropriate reservoir operation can significantly ease such situation.

Keywords A heuristic method; Socioeconomic drought index (SEDI); Climate change; VIC model; Reservoir operation; East River basin

1. Introduction

Drought is regarded as a complex natural hazard that occurs in large areas over long time periods and may have highly destructive effects on a number of aspects, such as water supply, agricultural production, and ecological environment (e.g., Gan et al., 2016; Yoo et al., 2016; Cammalleri et al., 2017). Generally, drought can be classified into four categories, including meteorological drought, agricultural drought, hydrological drought, and socioeconomic drought (Wilhite and Glantz, 1985; American Meteorological Society, 2013). Meteorological drought is often defined as a lack of precipitation over a region for a period of time; agricultural drought links various characteristics (e.g., soil moisture) of meteorological drought to agricultural impacts; hydrological drought is concerned with the effects of dry periods on surface or subsurface hydrology and water resources; socioeconomic drought is usually associated with supply of and demand for an economic good (water), which can also incorporate features of meteorological, agricultural, and hydrological droughts (Kifer and Steward, 1938; Wilhite and Glantz, 1985; Mishra and Singh, 2010). The former three have attracted the attentions of many researchers (e.g., Guttman, 1998; Heim, 2002; Narasimhan and Srinivasan, 2005; Shukla and Wood, 2008; Mishra and Singh, 2010; Morán-Tejeda et al., 2013; Moorhead et al., 2015; Serinaldi, 2016; Lin et al., 2017; Wu et al., 2017); however, to the best of our knowledge, it is only until

recently that there have been a few studies focusing on socioeconomic drought (e.g., Eklund and Seaquist, 2015; Mehran et al., 2015; Huang et al., 2016), which occurs when water resources systems cannot meet water demand due to a weather-related shortfall in water supply (American Meteorological Society, 2013). A drought can be quantified at different levels of water deficiency, but it is difficult to identify a drought event through comprehensively evaluating both water shortage and drought duration. Therefore, it is still a challenging task to develop such a new method and a new index for rationally identifying drought events.

In the past several decades, numerous drought indices have been developed based on different parameters (e.g., Heim, 2002; Mishra and Singh, 2010; Moorhead et al., 2015; Etienne et al., 2016; Ndehedehe et al., 2016). For example, Palmer (1965) proposed the Palmer Drought Severity Index (PDSI) based on precipitation, reference evapotranspiration and soil characteristics, which could be used for evaluating the meteorological anomaly at a variety of time scales; Karl (1986) further developed the Palmer Hydrological Drought Index (PHDI) to better treat the beginning and ending times of droughts. The Standardized Precipitation Index (SPI), originated by Mckee et al. (1993) based on only precipitation, is also a popular tool to investigate drought occurrence. Sivakumar et al. (2011) developed the Relative Water Deficit (RWD) using actual and potential evapotranspiration as inputs. Moreover, drought indices, such as Crop Moisture Index (CMI) (Palmer, 1968), Surface Water Supply Index (SWSI) (Shafer and Dezman, 1982), Vegetation Condition Index (VCI) (Kogan, 1995), and Standardized Precipitation-Evapotranspiration Index (SPEI) (Vicente-Serrano et al., 2010), are all widely-used. However, all the above indices are used for assessing the effects of meteorological (e.g., PDSI, SPI and SPEI), hydrological (e.g.,

84 PHDI and SWSI) and agricultural (e.g., CMI, RWD and VCI) droughts. Moreover, these
85 indices may have their own advantages and disadvantages. For example, SPI can be
86 calculated for a variety of time scales, but the length of precipitation record and nature of
87 probability distribution play a vital role in calculating SPI. PDSI is the first comprehensive
88 index to assess the total moisture status of a region, but some rules (e.g., assuming that all
89 precipitation is rain) to establish PDSI are arbitrary and PDSI is sensitive to precipitation
90 and temperature (Mishra and Singh, 2010). SWSI is regarded to be complementary to
91 PDSI, which has the synonymous scale with that used for PDSI and can monitor the
92 impacts of hydrological droughts on urban and industrial water supplies, irrigation and
93 hydroelectric power generation; however, the weights of the factors may vary with spatial
94 scales and temporal scales due to differences in hydroclimatic variability (Wilhite and
95 Glantz, 1985; Heim, 2002; Mishra and Singh, 2010). CMI is used as an indicator of the
96 availability of moisture to meet short-term crop needs, but there is unnatural response to
97 changes in temperature because of the dependence of the abnormal evapotranspiration term
98 on the magnitude of potential evapotranspiration (Juhasz and Kornfield, 1978; Wilhite and
99 Glantz, 1985; Mishra and Singh, 2010).

100 Due to continuous population growth, water demand has increased multifold and will
101 keep increasing in future, probably causing more socioeconomic drought events around the
102 world (Chen et al., 2016; Smirnov et al., 2016; Trinh et al., 2017). For this category of
103 drought which is the least investigated, Mehran et al. (2015) proposed the Multivariate
104 Standardized Reliability and Resilience Index (MSRRI) for assessing water stress due to
105 both climatic conditions and local reservoir levels, and Huang et al. (2016) applied this
106 index to examine the evolution characteristics of socioeconomic droughts in the Heihe

River basin in China. However, this index only focuses on water shortage but does not include drought duration, which may also have crucial influences on drought analysis. Thus, it is vital to develop a new index for identifying socioeconomic drought events through integrating both water shortage and drought duration, especially in the context of climate change.

Climate change has been recognized as one of the major factors that have great impacts on drought (e.g., Hanson and Weltzin, 2000; Aherne et al., 2006; Hirabayashi et al., 2008; Ahn et al., 2016; Gizaw and Gan, 2017; Linares et al., 2017; Tietjen et al., 2017). Even a small change in climate may cause a dramatic change in hydrological cycle, leading to more frequent hydrological extremes (e.g., Pilling and Jones, 2002; Chen et al., 2011; Vicuna et al., 2013; Gu et al., 2015; Shi and Wang, 2015; Hoang et al., 2016; Shi et al., 2016a, 2017a). Globally, IPCC (Intergovernmental Panel on Climate Change) (2013) reported that the averaged land and ocean surface temperature had a warming of 0.85 °C over the period of 1880-2012 and a fast warming trend of 0.12 °C/decade over the period of 1951-2012. Regionally, a remarkable warming trend has been found in South China (e.g., Chen et al., 2011; Chan et al., 2012; Lau and Ng, 2013). Fischer et al. (2013) projected climate extremes in the Pearl River basin for the period of 2011-2050 using the daily output from the regional climate model COSMO-CLM, and the results indicated that warmer and drier conditions could be expected in the western and eastern parts, especially in summer and autumn.

In recent years, we have conducted several studies on climate change over the Pearl River basin (e.g., Niu, 2013; Niu and Chen, 2014, 2016; Niu et al., 2014, 2015, 2017). Niu and Chen (2014) investigated the terrestrial hydrological responses to precipitation

variability over the West River basin with emphasis on an extreme drought event. Niu et al. (2014) revealed that the teleconnections between two climatic patterns (El Niño-Southern Oscillation, ENSO, and Indian Ocean Dipole, IOD) and hydrological variability, served as a reference for inferences on the occurrence of extreme hydrological events over the Pearl River basin. Niu et al. (2015) examined the spatio-temporal and evolution features of drought events over the West River basin, and showed the differences of meteorological, hydrological and agricultural droughts.

Based on the above previous studies, this study aims to develop a new method, a heuristic method, and a new index, socioeconomic drought index (SEDI), for identifying socioeconomic drought events on different severity levels (i.e., slight, moderate, severe and extreme) through comprehensively evaluating the impacts of both water shortage and drought duration under climate change. Considering the gap between water supply and water demand, streamflow is adopted as the principal input in the new method and index. Historical drought analysis is conducted using the observed data, which can validate the applicability of the new method and index, and future drought analysis is conducted using different datasets of climate change scenarios, which can reflect a variety of drought conditions in future. Moreover, the impact of dam (and related reservoir) construction on drought analysis will be discussed in this study. Overall, the proposed method and index (SEDI) can provide a better understanding of socioeconomic drought under climate change, which will be valuable for decision-makers to synthetically evaluate the impacts of climate change and hydraulic structures on water resources management.

2. Methodology

2.1. The heuristic method and the SEDI

For a designated river basin, the heuristic method and the SEDI are developed as follows (see Fig. 1). First, the minimum in-stream water requirement (noted as MWR hereafter) (see subsection 2.2 for details) of the river basin, which is enough to sustain and support the different functions in this river basin, is adopted as the threshold value through comprehensively considering a number of factors such as water quality, ecology, navigation, water supply and so on. Second, the monthly streamflow data, either the observed data recorded at the hydrological stations or the simulated data derived from the Variable Infiltration Capacity (noted as VIC hereafter) model (Liang et al., 1994) (see subsection 2.3 for details), are used to identify drought month. Then, the monthly difference, which is the monthly streamflow data minus the MWR, is calculated. In this study, if the monthly difference is smaller than 0 (i.e., water deficit), the corresponding month will be regarded as a drought month. Third, according to the cumulative water deficit derived from the monthly water deficit, drought duration (i.e., the number of continuous drought months) and water shortage (i.e., the largest cumulative water deficit during the drought period) can be identified. It is worth noting that a socioeconomic drought event will continue until the cumulative water deficit turns into a non-negative value. Finally, for each identified socioeconomic drought event, the SEDI value can be calculated through integrating the impacts of water shortage and drought duration, which are classified into four different levels (see Table 1). It is worth noting that the indicators related to experiment procedures (e.g., the MWR value) may vary with land use and land cover dynamic, catchment geomorphology and scale, and even some climate-related events occurred in a particular region. Therefore, the proposed method and index are region-

dependent, which indicates that the values of the indicators should be recalculated for different regions.

In this study, the four drought duration levels (DDLs) are defined as follows. The DDL value will be 1, 2, or 3 if the identified drought event is at the quarterly (i.e., 1-3 months), semi-annual (i.e., 4-6 months) or annual (i.e., 7-12 months) scale, respectively, and the DDL value will be 4 if the identified drought event lasts for more than a year (Table 1). In addition, the four water shortage levels (WSLs) are defined by a typical reservoir storage percentage (noted as RSP hereafter). In this study, the typical reservoir storage (noted as TRS hereafter) refers to the total manageable storage capacity of the reservoirs in a study area, and then the RSP can be calculated as the absolute value of the largest cumulative water deficit (noted as LCWD) divided by the TRS (Denver Water, 2002).

$$RSP = \frac{Abs\left(LCWD\right)}{TRS} \tag{1}$$

where Abs( ) is the function of taking the absolute value. The WSL value will be 1, 2, or 3 if the RSP value is less than 40%, 60% or 80%, respectively, and if the RSP value is larger than 80%, the WSL value will be 4 (Table 1).

Therefore, for each identified socioeconomic drought event, the SEDI is defined in terms of the DDL and WSL values (see the equation below).

$$SEDI = \max\left\{DDL, WSL\right\} \tag{2}$$

For example, if the WSL and DDL values are 2 and 3, the SEDI value will be 3, which means it is a severe socioeconomic drought event (Table 1). Fig. 2 shows the ranges of different SEDI values classified by different levels of water shortage and drought duration.

196 Consequently, historical and future drought analyses can be conducted based on the
197 proposed heuristic method and the SEDI.

198 Furthermore, to discuss the impact of reservoir operation on drought analysis, the
199 following method is adopted. For a designated reservoir, there should be an upper bound of
200 stored water (e.g., the effective storage of the reservoir) during the flood season limited by
201 the requirement of flood control, which is also the available water volume remaining in the
202 reservoir at the end of the flood season. Then, using the previously obtained monthly
203 differences, the available water volume in the reservoir at the end of each month can be
204 calculated by subtracting the monthly difference of that month from the available water
205 volume in the reservoir at the end of the last month. In this study, if the available water
206 volume turns into a negative value, it indicates that there will not be sufficient water even
207 if the usable capacity (e.g., the effective storage) of the reservoir is run out.

208 ***2.2. The MWR value***

209 The MWR is a critical variable in determining the drought occurrence and duration, and its
210 value can be calculated as follows (Wu and Chen, 2013):

211 $$MWR = \max\{Q_1, Q_2, Q_3, Q_4\} + Q_s \quad (3)$$

212 where Q_1 is the minimum streamflow required for maintaining water quality standard, Q_2
213 is the minimum ecological streamflow, Q_3 is the minimum streamflow for navigation, and
214 Q_4 is the minimum streamflow for arresting seawater intrusion into the estuary. Q_s is the
215 required pumping rate for the water supply to meet the regional water demand. In this
216 study, Q_s is estimated using a five-stage water demand projection model proposed by
217 Chen et al. (2015), which can project the future water demand in a designated region under

the high, medium, and low projection scenarios, respectively. This five-stage model uses the per capita gross domestic product based on purchasing power parity (noted as PPP GDP hereafter) and population as the main indicators to project future water demand. The PPP GDP serves as the indicator to identify the historic, current, and future water demand stages, which is the guide for water demand patterns, and population serves as the most important influencing factor for total water demand. Then, the regression equations to estimate the future water demand can be obtained (Chen et al., 2015). It is worth noting that the reasonable threshold value for the utilization ratio of water resources of a river is 30%, and the limiting threshold value is 40% (UN, 1997; Zuo, 2011). In other words, if more than 40% of river discharge is utilized, a critical situation regarding water scarcity exists whilst making use of less than 30% of river discharge can be regarded as sustainable and acceptable. As a result, the value of Q_s should not be larger than 30% of river discharge.

2.3. VIC model

One of representative land surface hydrological models, the VIC model (Liang et al., 1994), is a semi-distributed model, which maintains both surface energy and water balances over a grid cell, with its resolutions ranging from a fraction of a degree to several degrees latitude by longitude. The application of the sub-gird parameterization of the spatial variability of infiltration capacity in the VIC model makes it possible to represent the land surface hydrological processes at higher horizontal resolutions.

The VIC model has been applied to several large river basins (e.g., Nijssen et al., 2001). The high temporal resolution model forcing datasets and the global soil and vegetation datasets facilitate simulations and assessments of the global and regional land surface

241 hydrological processes by the VIC model. The characteristics of global surface soil
242 moisture fluxes at daily scale for the period of 1979-1993 were explored by the VIC model
243 (Nijssen et al., 2001). The VIC model was applied to the East River basin for exploring the
244 land surface hydrological features (Chen and Wu, 2008). Niu and Chen (2010) validated
245 the streamflow simulations in the Pearl River basin with the streamflow observations from
246 six hydrologic stations. Furthermore, Niu et al. (2014) further validated the streamflow
247 simulations in the Pearl River basin with the streamflow observations from four more
248 hydrologic stations. Overall, the VIC simulation of streamflow over the Pearl River basin
249 is comparable to the observations. As a result, the parameters in the VIC model and the
250 related routing model, which can be acquired from the previous studies (Chen and Wu,
251 2008; Niu and Chen, 2010; Niu et al., 2014), are directly used to simulate the future
252 streamflow using climate projection scenarios which are downscaled from the outputs of
253 General Circulation Models (GCMs) in this study. It is worth noting that there is no need
254 to calibrate the VIC model for simulations at the monthly scale, with the acceptable
255 simulation accuracy in the study basin. For running the VIC model, the soil and vegetation
256 parameters are extracted from two global datasets (Nijssen et al., 2001).

257 ***2.4. Trend test method***

258 In order to investigate the trends of the simulated future streamflow using different climate
259 change scenarios, the Mann-Kendall trend test method is adopted. A number of previous
260 studies have shown the robustness of this method as well as its wide application in the
261 fields such as meteorology, hydrology, and sedimentology (e.g., Croitoru et al., 2012;
262 Manzanas et al., 2014; Shi and Wang, 2015; Shi et al., 2016b, 2017b).

The Mann-Kendall trend test is a non-parametric rank-based statistical test that was first proposed by Mann (1945) and further developed by Kendall (1975). Based on the Mann-Kendall trend test method, the slope of the series can be computed using the Thiel-Sen method (Thiel, 1950; Sen, 1968).

$$\beta = Median\left(\frac{X_j - X_i}{j - i}\right),\ for\ all\ i < j \tag{4}$$

where X_j and X_i are the observed values in the j-th and i-th year ($j > i$), respectively.

Moreover, prewhitening (von Storch and Navarra, 1995) is required to eliminate the influence of autocorrelation because such series is not applicable for the Mann-Kendall trend test method.

$$Xp_i = X_{i+1} - rX_i \tag{5}$$

where Xp_i is the observed value in the i-th year after prewhitening and r is the first-order autocorrelation coefficient of the series.

3. Study area and research data

3.1. Study area

The study area is the East River, a tributary of the Pearl River, which is the most important source of fresh water for Hong Kong (Niu and Chen, 2010). Therefore, to explore the status of water resources in this river basin is essential for evaluating water security of Hong Kong. The East River originates in the Xunwu county of Jiangxi Province, China, and its drainage area is 27040 km^2, accounting for 5.96% of the total area of the Pearl River basin (PRWRC, 2005). The main stream of the East River flows from northeast to

283 southwest (see Fig. 3), and the long-term annual average discharge in the East River is
284 23.8 km^3 (~ 755 m^3/s). The upper reach, named the Xunwushui River, flows towards the
285 southwest and joins the Anyuanshui River in the Longchuan County, and from thereon it is
286 named the East River. It is worth noting that the river channel in the mountainous upstream
287 area of the East River is shallow and narrow, while the river channels in the middle and
288 downstream areas can be used for navigation. Moreover, the Xinfengjiang (noted as XFJ
289 hereafter) Reservoir, a multi-year reservoir located in the East River basin, was completed
290 in 1962. The total reservoir storage capacity is 13.9 km^3, among which 3.1 km^3 is the flood
291 control storage, 6.5 km^3 is the effective storage, and 4.3 km^3 is the dead storage (Wu and
292 Chen, 2012, 2013). In our previous studies, Niu (2013) examined the temporal patterns of
293 precipitation and the influence of large-scale climate, and found a number of abnormal
294 precipitation events during 1955-1975, 1980-1985, and 1990-1995 in the East River basin.
295 Moreover, regarding dam (and related reservoir) construction as the best option to increase
296 available water resources by storing water in the reservoir and to enhance the capabilities
297 in water resources management (Chen et al., 2016), we have also proposed an operation-
298 based scheme for a multi-year and multi-purpose reservoir (Wu and Chen, 2012), an
299 improved method for irrigation water demand estimation, and an optimization method for
300 reservoir operation (Wu and Chen, 2013).

301 ***3.2. Research data***

302 In this study, the projected precipitation datasets derived from different climate change
303 scenarios are the outputs from 17 GCMs, including 16 IPCC AR4 (the Fourth Assessment
304 Report) GCMs during 1951-2099 and 1 IPCC AR5 (the Fifth Assessment Report) GCM
305 during 2000-2099 (see Table 2). The selected AR4 GCMs used three scenarios (Special

306 Report on Emissions Scenario, SRES A2/A1B/B1) to project future climate change, and
307 assumptions were made about how factors driving emissions (e.g., population growth,
308 economic development and advances in technology) would change in future (IPCC, 2007).
309 Moreover, the selected AR5 GCM adopted four new scenarios (Representative
310 Concentration Pathway, RCP 2.6/4.5/6.0/8.5). Instead of making assumptions about how
311 factors driving emissions might change, each RCP scenario expressed a different total
312 radiative forcing by 2100 or how much extra energy the earth would retain as a result of
313 human activities (IPCC, 2013). The GCM outputs can be obtained from the World Climate
314 Research Programme (WCRP) CMIP3 multi-model dataset (Meehl et al., 2007). These
315 data have been downscaled to a 0.5° grid using the bias-correction/spatial downscaling
316 method (Wood et al., 2004; Maurer et al., 2009), based on the gridded observations during
317 1950-1999 (Adam and Lettenmaier, 2003). With the 52 (=16×3+4) projected precipitation
318 datasets, the monthly streamflow data used for drought analysis can be simulated using the
319 VIC model. In addition, the observed monthly streamflow data recorded at the Boluo
320 station (see Fig. 3) in the East River basin during 1954-1988 are collected.

321 To delineate the East River basin, GTOPO30 DEM dataset with 1000 m spatial
322 resolution is used (see Fig. 3). The VIC model is run at the daily scale with 0.5°×0.5°
323 spatial resolution to provide the simulated streamflow, and the soil and vegetation data
324 over this river basin are extracted from the global soil and vegetation datasets (Nijssen et
325 al., 2001).

326 ## 4. Results and discussion

4.1. The MWR value of the East River basin

For the East River basin, the MWR value is calculated through considering the change of water demand in future. Following the previous studies (Wu et al., 2001; Lee et al., 2007), this study adopts the estimated values of Q_1, Q_2, Q_3, and Q_4 at the Boluo station as 317, 230, 210, and 150 m^3/s in 2010, respectively. Further, this study assumes that these values will not change along with time; therefore, the maximum value among Q_1, Q_2, Q_3, and Q_4 is 317 m^3/s. According to Lee et al. (2007), the estimated value of Q_s was 150 m^3/s in 2010; however, it is worth noting that water demand will increase along with population growth in future (Chen et al., 2016), leading to the change of the Q_s value, as well as the MWR value. Chen et al. (2015) projected the future water demand in the East River basin under the high, medium and low projection scenarios using a five-stage water demand projection model, and the results showed that the annual water demand would keep increasing before 2070 and then decrease from 2070 to 2099 under the high and medium projection scenarios. According to the above mentioned assumption, the MWR value will have the same changing feature with the annual water demand in future. As a result, the MWR value of the East River basin for each year during 2010-2099 can be obtained (Fig. 4). In this study, the MWR values under the medium projection scenario from 2020 to 2099 are selected for future drought analysis, and the maximum Q_s value under this scenario (176 m^3/s) will occur in 2070. Because the long-term annual average river discharge in the East River is 755 m^3/s, the maximum Q_s value under this scenario accounts for 23.3% (= 176/755) of the total river discharge, which can meet the requirement of less than 30% (Zuo, 2011).

4.2. Historical drought analysis

Due to data availability, the observed monthly streamflow data recorded at the Boluo station in the East River basin during 1954-1988 are collected in this study. Moreover, only the monthly streamflow data simulated using the 48 (=16×3) datasets from 16 GCMs and 3 AR4 scenarios are used for historical drought analysis. Fig. 5 shows the comparison of the mean value of the simulated streamflow data from the 48 datasets against the observations for each month during 1954-1988. Overall, the average values of the simulated streamflow data from the 48 datasets can match the historical observations; however, large differences appear in a few months. The reasons for this may be as follows: on the one hand, the monthly streamflow at the Boluo station is significantly influenced by the operation of the XFJ Reservoir (Niu and Chen, 2010; Wu and Chen, 2012), and Niu and Chen (2010) indicated that the model performance of streamflow simulation is satisfied before the operation of the XFJ Reservoir. On the other hand, in climate change study, the GCM outputs can be used to analyze natural multi-decadal climate variations, but cannot be used to confirm the exact extreme events occurred in a certain year (Teegavarapu, 2012).

Using the heuristic method and the SEDI proposed in subsection 2.1, historical socioeconomic drought events are identified from the observed and simulated monthly streamflow data, respectively. For the observed monthly streamflow data, the SEDI value of the severest drought event over the period of 1954-1988 is 4, which can reach the level of an extreme drought. The identified socioeconomic drought event started in December 1962 and ended in May 1964, lasting for 18 months (i.e., DDL=4); however, the RSP value of this drought event is only 0.37 (i.e., WSL=1). In addition, based on the simulated

monthly streamflow data, the SEDI value of the severest drought event over the period of 1954-1988 is 3, which indicates this is a severe drought. The identified socioeconomic drought event started in September 1962 and ended in May 1963, lasting for 9 months (i.e., DDL=3); moreover, the RSP value of this drought event is 0.61 (i.e., WSL=3). According to the historical records, the severest drought event during 1954-1988 indeed occurred around 1963 (Peart, 2004), which preliminarily proves the validity of the heuristic method and the SEDI for identifying the occurrence period of the socioeconomic drought event. However, the drought duration of the socioeconomic drought event identified from the observed data is longer, but the water shortage of the socioeconomic drought event identified from the simulated data is higher.

4.3. Future drought analysis

4.3.1. Trend analysis of the simulated streamflow in future

In this study, trend analysis of the simulated streamflow at the Boluo station during 2020-2099 is conducted at the annual scale. Using the Mann-Kendall trend test method, the trends of the annual streamflow data under all the 52 datasets are detected and Table 3 lists the relevant results. The trend slopes vary greatly among different scenarios, with the most significant decreasing trend of -2.77 mm/year in one GCM (i.e., mpi_echam5.1) under A1B scenario and the most significant increasing trend of 11.02 mm/year in another GCM (i.e., ukmo_hadcm3.1) under B1 scenario. There are 40 AR4 datasets (i.e., 12/13/15 under A1B/A2/B1 scenarios) showing the increasing trends in the simulated annual streamflow, comparing to only 8 AR4 datasets (i.e., 4/3/1 under A1B/A2/B1 scenarios) showing the decreasing trends. However, 20 of the 40 (i.e., 50%) increasing trends are statistically significant (p<0.1) while only 1 of the 8 (i.e., 12.5%) decreasing trends is statistically

395 significant. In contrast, the increasing trends are found under all the four AR5 datasets,
396 among which only the increasing trend under RCP 4.5 scenario is not statistically
397 significant (see Table 3).

398 It is worth noting that more datasets show the increasing trends rather than the
399 decreasing trends in the simulated streamflow at the annual scale. However, it does not
400 mean that the drought conditions will be improved in future because of the non-uniformity
401 of the streamflow among different months. In the following subsection, future drought
402 analysis will be conducted at the monthly scale, focusing on the identification of
403 socioeconomic drought events.

404 *4.3.2. Identification of socioeconomic drought events in future*

405 In consideration of the changing MWR values of the East River basin under medium
406 projection scenarios during 2020-2099 (Fig. 4), socioeconomic drought events in future are
407 identified based on the monthly streamflow data simulated with 16 GCMs under the three
408 AR4 emission scenarios and 1 GCM under the four AR5 scenarios.

409 First, the numbers of socioeconomic drought events with different SEDI values are
410 identified for each of the 52 datasets, and the results are shown in Fig. 6. For the 16 GCMs,
411 the results are rather different among different models under the three AR4 emission
412 scenarios (i.e., SRES A1B/A2/B1). The total numbers of socioeconomic drought events
413 vary between 85~114 under SRES A1B scenario, 84~120 under SRES A2 scenario and
414 91~115 under SRES B1 scenario, respectively. The mean values of the total numbers are
415 more or less the same under the three emission scenarios (i.e., 100, 99 and 102 under
416 SRES A1B, A2 and B1 scenarios, respectively). For the four AR5 scenarios (i.e., RCP
417 2.6/4.5/6.0/8.5) of the 1 GCM, the variations of 93-98 are found for the total numbers of

418 socioeconomic drought events, and the mean value of the total numbers is 96, which is a
419 little smaller than those from the 16 AR4 GCMs. Moreover, the extreme socioeconomic
420 drought events (i.e., SEDI=4) will only account for a small percentage under all the 52
421 datasets, and the overall percentages of extreme socioeconomic drought events are 11%
422 and 1% for the 16 AR4 GCMs and the 1 AR5 GCM, respectively. Regarding severe
423 socioeconomic drought events (i.e., SEDI=3) in future, the overall percentages are 35%
424 and 55% for the 16 AR4 GCMs and the 1 AR5 GCM, respectively. As mentioned before,
425 the GCM outputs can be used to analyze multi-decadal climate variations rather than to
426 give the exact occurrence period of a drought event (Teegavarapu, 2012); therefore, the
427 identified drought periods are for reference only. For example, an extreme socioeconomic
428 drought event (i.e., SEDI=4) is identified in 2079-2080 under RCP 8.5 scenario; it can only
429 be inferred that there might be an extreme socioeconomic drought event during 2020-2099;
430 however, the exact occurrence period of this event might be in other years rather than in
431 2079-2080.

432 Second, for each of the 52 datasets, the socioeconomic drought event with the longest
433 drought duration in future is identified (see Fig. 7). It is observed that the values of the
434 longest drought duration identified from the AR4 GCMs are generally larger than those
435 identified from the AR5 GCM. The mean value of the longest drought duration identified
436 from the AR4 GCMs is 33 months, and specially, the socioeconomic drought event
437 identified from one AR4 GCM (i.e., csiro_mk3_0.1) under A1B scenario will last for 93
438 months (nearly 8 years), which is rather a long time. Moreover, the RSP value of this event
439 is 3.05, indicating that there will be a desperate water shortage during that period. Known
440 from Table 3, a decreasing trend in the simulated annual streamflow can be detected under

441 this scenario, which may partly explain this situation. In contrast, the mean value of the
442 longest drought duration identified from the AR5 GCM is only 14 months, much smaller
443 than that identified from the AR4 GCMs, and the longest drought durations are 13, 12, 21
444 and 11 under RCP 2.6, 4.5, 6.0 and 8.5 scenarios, respectively. It indicates that, compared
445 to the 16 AR4 GCMs, the selected 1 AR5 GCM will estimate future drought with a more
446 optimistic view from the aspect of drought duration. In addition, the values of the longest
447 drought duration identified from the 52 datasets are all larger than 9 months, which is the
448 drought duration of the 1963 drought event identified from the simulated streamflow data.

449 Third, with reference to water shortage which is also a crucial factor, the largest RSP
450 value under each of the 52 datasets is listed in Table 4. For the 16 AR4 GCMs, the largest
451 RSP values vary between 0.91~2.53 under SRES B1 scenario, 0.91~3.05 under SRES A1B
452 scenario and 0.94~2.39 under SRES A2 scenario, respectively, and the mean values under
453 these three SRES scenarios are 1.49, 1.62 and 1.89, respectively. For the 1 AR5 GCM, the
454 largest RSP values are 0.69, 0.77, 0.82 and 0.86 under RCP 2.6, 4.5, 6.0 and 8.5 scenarios,
455 respectively. As a result, even the worst situation derived from the 1 AR5 GCM (i.e., 0.86)
456 is better than the best situation derived from the 16 AR4 GCMs (i.e., 0.91), which indicates
457 that, compared to the 16 AR4 GCMs, the selected 1 AR5 GCM will estimate future
458 drought with a more optimistic view from the aspect of water shortage, which is the same
459 as the result from the analysis of drought duration.

460 Conclusively, Table 5 lists the number of socioeconomic drought events with either
461 longer duration or larger RSP value than the 1963 drought event identified from the
462 simulated streamflow data during 2020-2099 for each of the 52 datasets, and the
463 percentage in the parentheses is calculated by dividing the total number of socioeconomic

464 drought events for the corresponding dataset. For the 16 AR4 GCMs, the numbers of such
465 events vary between 16~39 under SRES A1B scenario, 18~39 under SRES A2 scenario
466 and 22~39 under SRES B1 scenario, respectively. In future, socioeconomic drought events
467 severer than the 1963 drought event will account for about 31% of the total. In contrast, for
468 the four RCP scenarios (i.e., RCP 2.6/4.5/6.0/8.5) of the 1 AR5 GCM, smaller variations
469 are found for the numbers of socioeconomic drought events severer than the 1963 drought
470 event (i.e., 7~11), and the percentage of such events is about 9%, which once again proves
471 the previous conclusion that the future drought condition estimated by the selected 1 AR5
472 GCM will be more optimistic than that estimated by the 16 AR4 GCMs.

473 ***4.4. Impact of the XFJ Reservoir***

474 In the previous subsection, a number of socioeconomic drought events with different SEDI
475 values have been identified in the East River basin. Therefore, serious water scarcity will
476 be most likely to occur, especially if proper planning, development and management
477 strategies are not adopted. For much of the 20th century, dam construction is regarded as
478 the best option to increase available water resources by storing water in the reservoir and
479 enhance the capabilities in water resources management (Wu and Chen, 2012, 2013; Chen
480 et al., 2016). Fortunately, a multi-year reservoir, the XFJ Reservoir, was completed in 1962
481 in the East River basin. Wu and Chen (2012) indicated that the usable capacity of the XFJ
482 Reservoir was 5.8-6.5 km^3, which implied that at least nearly 90% of the effective storage
483 (i.e., 6.5 km^3) of the XFJ Reservoir would be used to store water in the flood season. This
484 study adopts 5.8 km^3 as the TRS for the East River basin, which is 0.89 (=5.8/6.5) of the
485 total effective storage, as the usable capacity (i.e., the available water volume) in the XFJ
486 Reservoir when the flood season ends.

The monthly streamflow data simulated using the 52 datasets are used to analyze the impact of the XFJ Reservoir on future drought for the period of 2020-2099. Using the method described in subsection 2.1, the available water volume in the XFJ Reservoir at the end of each month during 2020-2099 can be calculated. For the selected 1 AR5 GCM, without the reservoir, the largest RSP value under the four scenarios is 0.86 (see Table 4), which is smaller than 0.89; it indicates that the usable capacity (5.8 km^3) of the XFJ Reservoir is sufficient to cover the largest cumulative water deficit. However, for the 16 AR5 GCMs, with the reservoir, even the smallest RSP value (i.e., 0.91) in Table 4 is larger than 0.89, which means that water deficits will still remain in certain periods even if the adopted usable capacity is run out.

Fig. 8 shows the monthly available water volume in the XFJ Reservoir during 2020-2099 under three representative scenarios, namely, RCP 8.5 scenario with the largest RSP value of 0.86 (HadGEM2-ES), SRES A1B scenario with the largest RSP value of 1.11 (ukmo_hadcm3.1) and SRES B1 scenario with the largest RSP value of 1.40 (ipsl_cm4.1). The red dash lines denote that the usable capacity of the XFJ Reservoir (i.e., 5.8 km^3) is run out. For RCP 8.5 scenario (HadGEM2-ES), the usable capacity of the XFJ Reservoir will be sufficient for future water demand (see Fig. 8a), For SRES A1B scenario (ukmo_hadcm3.1) and SRES B1 scenario (ipsl_cm4.1), there are several drought events whose water deficits cannot be completely tackled by the usable capacity of the XFJ Reservoir (see Figs. 8b and 8c).

Furthermore, it is worth noting that the available water volume in the XFJ Reservoir at the end of the flood season is usually less than 5.8 km^3, which will have a great influence on future drought analysis. Therefore, relationship between the number of socioeconomic

510 drought events and the used percentage of the effective storage of the XFJ Reservoir is
511 discussed, taking the 1 AR5 GCM under the four RCP scenarios during 2020-2099 as a
512 case study, and the relevant results are shown in Fig. 9 and Table 6. Along with the
513 increase of the used percentage of the effective storage, the total number of socioeconomic
514 drought events will monotonously decrease under all these four scenarios; however, the
515 decreasing trends can be divided into three phases, with quite different decreasing features.
516 Since the step of the used percentage for this analysis is 10%, the first cutoff point is found
517 between 20% and 30% while the second cutoff point is found between 60% and 70% (see
518 Fig. 9). When no more than 20% of the effective storage is used, the average trend slope
519 for all these four scenarios is -0.94 (R^2 = 0.85), which is much weaker than that (i.e., -2.08,
520 R^2 = 0.96) when the used percentage is between 30% and 60%. Moreover, when no less
521 than 70% of the effective storage is used, the decreasing trend becomes quite weak (i.e., -
522 0.11, R^2 = 0.48) mainly because the total number of socioeconomic drought events is small.
523 As a result, to reserve 70% of the effective storage of the XFJ Reservoir at the end of the
524 flood season can be a good option because most socioeconomic drought events will be
525 overcome in that case. In addition, regarding the number of socioeconomic drought events
526 with different SEDI values (see Table 6), when no less than 30% of the effective storage is
527 used, most socioeconomic drought events on severe (i.e., SEDI=3) and extreme (i.e.,
528 SEDI=4) levels will be removed. For example, when the used percentage is 30%, there will
529 be no extreme socioeconomic drought events during 2020-2099, and only 2, 3, 3, and 6
530 severe socioeconomic drought events are remaining under these four RCP scenarios,
531 respectively. Consequently, for the climate change circumstances provided by the 1 AR5

GCM, we would suggest to reserve at least 30% of the effective storage of the XFJ Reservoir at the end of the flood season.

5. Conclusions

This study proposes a new method (i.e., a heuristic method) and a new index (i.e., the SEDI) for identifying socioeconomic drought events on different severity levels under climate change through comprehensively evaluating the impacts of both water shortage and drought duration. Taking the East River basin in South China as the study area, this study analyzes both the historical and future socioeconomic drought events using the proposed method and index. The contributions of this study can be described as follows:

First, the MWR value of the East River basin for each year during 2010-2099 is obtained through considering the change of water demand in future, which can be a target of the integrated water resources management in this river basin and a reference to other river basins. Second, the SEDI is validated through historical drought analysis, and then applied to future drought analysis. The trends of the simulated streamflow derived from 52 datasets are analyzed, and socioeconomic drought events during 2020-2099 are identified. The results indicate that a number of socioeconomic drought events severer than the 1963 drought event may occur in future, which will be a great challenge for the society. Third, through analyzing the impact of the XFJ Reservoir on future droughts, this study indicates that most of the identified socioeconomic drought events can be mitigated by reservoir operation if the used percentage of the effective storage at the end of the flood season is 70%. Moreover, it is suggested that at least 30% of the effective storage should be reserved

553 in the XFJ Reservoir at the end of the flood season to overcome most of the severe and
554 extreme socioeconomic drought events.

555 Furthermore, applying the proposed method and index for identifying socioeconomic
556 drought events under climate change, we also need fully aware the following limitations,
557 which are mainly related to five aspects. First, one important indicator to develop the SEDI
558 is the RSP, in which the effective reservoir storage is a necessary variable. Therefore, the
559 heuristic method and the SEDI are inapplicable to river basins without reservoir operation.
560 Fortunately, reservoir seems to be the requisite infrastructure in river basins where
561 socioeconomic drought events may occur because reservoir can definitely enhance the
562 capabilities in meeting water demand (Chen et al., 2016). Second, the proposed method
563 and index are region-dependent. The study area is located in a humid region, and the
564 method and index are applicable. For arid or semi-arid regions, more water-related factors
565 (e.g., utilization of groundwater) besides streamflow may have to be considered, and the
566 method and index may need more validations. Nevertheless, the proposed method and
567 index may interpret the occurrence of drought event in arid or semi-arid regions from the
568 perspective of water supply and demand, rather than only from the perspective of
569 climatology. Moreover, for different regions, relationship between the number of
570 socioeconomic drought events and the used percentage of the effective storage should be
571 reestablished and suggestion about the used percentage of the effective storage may be
572 different. Third, this study adopts the simulation results of a semi-distributed model (i.e.,
573 the VIC model) over a relatively coarse resolution spatial grid, which may simplify the
574 description of the behavior of spatially distributed physical systems and may bring in
575 errors. Distributed hydrological models can be used in the future work to further analyze

the possible influences of different models on the proposed method and index. Fourth, the missing data will influence the computation of the SEDI. Nevertheless, this study uses the simulated streamflow from the VIC model, and there is no missing data. Fifth, it is worth noting that IPCC is still intensively monitoring and studying climate change and new climate change projections will be issued in the next several years. Therefore, the performance of the proposed method and index should be re-evaluated when the new systematic projections are available.

Nevertheless, with the awareness of the above limitations, the heuristic method and the SEDI proposed in this study can provide a new avenue of identifying socioeconomic drought events under climate change, which would be valuable for sustainable water resources management. It is worth noting that the proposed new method and index would be promising in other humid regions with reservoir operation around the world. Even if in arid or semi-arid regions, the proposed new method and index can be regarded as a pilot exploration of understanding drought events from a socioeconomic perspective.

Acknowledgements

This study was supported by the Consultancy Services project for Water Supplies Department of Hong Kong "Study on impacts of climate change on the water resources of Hong Kong", the Natural Science Foundation of Qinghai Province project (Grant No. 2017-ZJ-911), and the Special Funding for Science and Technology Development in Guangdong Province (Grant No. 2016A050503035). We are also grateful to the two

anonymous reviewers and Associate Editor (Prof. Wei Ouyang) who offered the insightful and constructive comments leading to improvement of this paper.

References

Adam, J.C., Lettenmaier, D.P., 2003. Adjustment of global gridded precipitation for systematic bias. *Journal of Geophysical Research*, 108: 1-14.

Aherne, J., Larssen, T., Cosby, B.J., Dillon, P.J., 2006. Climate variability and forecasting surface water recovery from acidification: Modelling drought-induced sulphate release from wetlands. *Science of the Total Environment*, 365: 186-199.

Ahn, S.R., Jeong, J.H., Kim, S.J., 2016. Assessing drought threats to agricultural water supplies under climate change by combining the SWAT and MODSIM models for the Geum River basin, South Korea. *Hydrological Sciences Journal*, 61(15): 2740-2753.

American Meteorological Society, 2013. Drought - An Information Statement of the American Meteorological Society. https://www.ametsoc.org/ams/index.cfm/about-ams/ams-statements/statements-of-the-ams-in-force/drought/

Cammalleri, C., Vogt, J., Salamon, P., 2017. Development of an operational low-flow index for hydrological drought monitoring over Europe. *Hydrological Sciences Journal*, 62(3): 346-358.

Chan, H., Kok, M., Lee, T., 2012. Temperature trends in Hong Kong from a seasonal perspective. *Climate Research*, 55(1): 53-63.

Chen, J., Li, Q.L., Niu, J., Sun, L.Q., 2011. Regional climate change and local urbanization effects on weather variables in Southeast China. *Stochastic Environmental Research and Risk Assessment*, 25(4): 555-565.

Chen, J., Shi, H.Y., Sivakumar, B., Peart, M.R., 2016. Population, Water, Food, Energy and Dams. *Renewable and Sustainable Energy Reviews*, 56: 18-28.

Chen, J., Wu, Y.P., 2008. Exploring hydrological process features of the East River (Dongjiang) basin in South China using VIC and SWAT. *Proceedings of the International Association*

624 *of Hydrological Sciences and the International Water Resources Association Conference*,
625 Guangzhou, China, 8-10.
626 Chen, J., Xing, B.D., Shi, H.Y., Zhang, B., 2015. A new model for long-term global water demand
627 projection. *AGU Fall Meeting*, San Francisco, USA.
628 Croitoru, A.E., Holobaca, I.H., Lazar, C., Moldovan, F., Imbroane, A., 2012. Air temperature trend
629 and the impact on winter wheat phenology in Romania. *Climatic Change*, 111(2): 393-410.
630 Denver Water, 2002. *Water for Tomorrow: An Integrated Water Resource Plan.*
631 Eklund, L., Seaquist, J., 2015. Meteorological, agricultural and socioeconomic drought in the
632 Duhok Governorate, Iraqi Kurdistan. *Natural Hazards*, 76(1): 421-441.
633 Etienne, E., Devineni, N., Khanbilvardi, R., Lall, U., 2016. Development of a Demand Sensitive
634 Drought Index and its application for agriculture over the conterminous United States.
635 *Journal of Hydrology*, 534: 219-229.
636 Fischer, T., Menz, C., Su, B., Scholten, T., 2013. Simulated and projected climate extremes in the
637 Zhujiang River Basin, South China, using the regional climate model COSMO-CLM.
638 *International Journal of Climatology*, 33: 2988-3001.
639 Gan, T.Y., Ito, M., Hulsmann, S., Qin, X., Lu, X.X., Liong, S.Y., Rutschman, P., Disse, M.,
640 Koivusalo, H., 2016. Possible climate change/variability and human impacts, vulnerability
641 of drought-prone regions, water resources and capacity building for Africa. *Hydrological*
642 *Sciences Journal*, 61(7): 1209-1226.
643 Gizaw, M.S., Gan, T.Y., 2017. Impact of climate change and El Nio episodes on droughts in sub-
644 Saharan Africa. *Climate Dynamics*, 49(1-2): 665-682.
645 Gu, H.H., Yu, Z.B., Wang, G.L., Wang, J.G., Ju, Q., Yang, C.G., Fan, C.H., 2015. Impact of
646 climate change on hydrological extremes in the Yangtze River Basin, China. *Stochastic*
647 *Environmental Research and Risk Assessment*, 29(3): 693-707.

Guttman, N.B., 1998. Comparing the Palmer Drought Index and the standardized precipitation index. *Journal of the American Water Resources Association*, 34(1): 113-121.

Hanson, P.J., Weltzin, J.F., 2000. Drought disturbance from climate change: response of United States forests. *Science of the Total Environment*, 262(3): 205-220.

Heim, R.R., 2002. A review of twentieth-century drought indices used in the United States. *Bulletin of the American Meteorological Society*, 83: 1149-1166.

Hirabayashi, Y., Kanae, S., Emori, S., Oki, T., Kimoto, M., 2008. Global projections of changing risks of floods and droughts in a changing climate. *Hydrological Sciences Journal*, 53(4): 754-772.

Hoang, L.P., Lauri, H., Kummu, M., Koponen, J., van Vliet, M.T.H., Supit, I., Leemans, R., Kabat, P., Ludwig, F., 2016. Mekong River flow and hydrological extremes under climate change. *Hydrology and Earth System Sciences*, 20(7): 3027-3041.

Huang, S.Z., Huang, Q., Leng, G.Y., Liu, S.Y., 2016. A nonparametric multivariate standardized drought index for characterizing socioeconomic drought: A case study in the Heihe River Basin. *Journal of Hydrology*, 542: 875-883.

IPCC, 2007. Climate Change 2007: The Physical Science Basis. *Contribution of Working Group I to the Fourth Assessment Report of the IPCC*, Cambridge University Press, Cambridge, United Kingdom and New York, USA.

IPCC, 2013. Climate Change 2013: The Physical Science Basis. *Contribution of Working Group I to the Fifth Assessment Report of the IPCC*, Cambridge University Press, Cambridge, United Kingdom and New York, USA.

Juhasz, T., Kornfield, J., 1978. The Crop Moisture Index: unnatural response to changes in temperature. *Journal of Applied Meteorology and Climatology*, 17: 1864-1865.

671 Karl, T.R., 1986. The sensitivity of the Palmer Drought Severity Index and Palmer's Z-Index to
672 their calibration coefficients including potential evapotranspiration. *Journal of Climate and*
673 *Applied Meteorology*, 25: 77-86.
674 Kendall, M.G., 1975. *Rank Correlation Measures*. London: Charles Griffin.
675 Kifer, R.S., Steward, H.L., 1938. Farming hazards in the drought area. *Monograph XVI*,
676 Washington, DC: Works Progress Administration.
677 Kogan, F.N., 1995. Droughts of the late 1980s in the United States as derived from NOAA Polar-
678 Orbiting Satellite Data. *Bulletin of the American Meteorological Society*, 76: 655-668.
679 Lau, K.L., Ng, E., 2013. An investigation of urbanization effect on urban and rural Hong Kong
680 using a 40-year extended temperature record. *Landscape and Urban Planning*, 114: 42-52.
681 Lee, J.H.W., Wang, Z.Y., Thoe, W., Cheng, D.S., 2007. Integrated physical and ecological
682 management of the East River. *Water Science and Technology: Water Supply*, 7: 81-91.
683 Liang, X., Lettenmaier, D.P., Wood, E.F., Burges, S.J., 1994. A simple hydrologically based model
684 of land surface water and energy fluxes for general circulation models. *Journal of*
685 *Geophysical Research*, 99(D7): 14415-14428.
686 Lin, Q.X., Wu, Z.Y., Singh, V.P., Sadeghi, S.H.R., He, H., Lu, G.H., 2017. Correlation between
687 hydrological drought, climatic factors, reservoir operation, and vegetation cover in the
688 Xijiang Basin, South China. *Journal of Hydrology*, 549: 512-524.
689 Linares, R., Roque, C., Gutierrez, F., Zarroca, M., Carbonel, D., Bach, J., Fabregat, I., 2017. The
690 impact of droughts and climate change on sinkhole occurrence. A case study from the
691 evaporite karst of the Fluvia Valley, NE Spain. *Science of the Total Environment*, 579: 345-
692 358.
693 Mann, H.B., 1945. Non-parametric tests against trend. *Econometrica*, 13: 245-259.

694 Manzanas, R., Amekudzi, L.K., Preko, K., Herrera, S., Gutierrez, J.M., 2014. Precipitation
695 variability and trends in Ghana: An intercomparison of observational and reanalysis
696 products. *Climatic Change*, 124(4): 805-819.
697 Maurer, E.P., Adam, J.C., Wood, A.W., 2009. Climate model based consensus on the hydrologic
698 impacts of climate change to the Rio Lempa basin of Central America. *Hydrology and*
699 *Earth System Sciences*, 13: 183-194.
700 McKee, T.B., Doesken, N.J., Kleist, J., 1993. The relationship of drought frequency and duration to
701 time scales. *Eighth Conference on Applied Climatology*, American Meteorological Society,
702 Anaheim, California.
703 Meehl, G.A., Covey, C., Delworth, T., Latif, M., McAvaney, B., Mitchell, J.F.B., Stouffer, R.J.,
704 Taylor, K.E., 2007. The WCRP CMIP3 multi-model dataset: A new era in climate change
705 research. *Bulletin of the American Meteorological Society*, 88: 1383-1394.
706 Mehran, A., Mazdiyasni, O., AghaKouchak, A., 2015. A hybrid framework for assessing
707 socioeconomic drought: Linking climate variability, local resilience, and demand. *Journal*
708 *of Geophysical Research-Atmospheres*, 120(15): 7520-7533.
709 Mishra, A.K., Singh, V.P., 2010. A review of drought concepts. *Journal of Hydrology*, 391: 202-
710 216.
711 Moorhead, J.E., Gowda, P.H., Singh, V.P., Porter, D.O., Marek, T.H., Howell, T.A., Stewart, B.A.,
712 2015. Identifying and evaluating a suitable index for agricultural drought monitoring in the
713 Texas high plains. *Journal of the American Water Resources Association*, 51(3): 807-820.
714 Morán-Tejeda, E., Ceglar, A., Medved-Cvikl, B., Vicente-Serrano, S.M., López-Moreno, J.I.,
715 González-Hidalgo, J.C., Revuelto, J., Lorenzo-Lacruz, J., Camarero, J., Pasho, E., 2013.
716 Assessing the capability of multi-scale drought datasets to quantify drought severity and to
717 identify drought impacts: an example in the Ebro Basin. *International Journal of*
718 *Climatology*, 33(8): 1884-1897.

719 Narasimhan, B., Srinivasan, R., 2005. Development and evaluation of Soil Moisture Deficit Index
720 (SMDI) and Evapotranspiration Deficit Index (ETDI) for agricultural drought monitoring.
721 *Agricultural and Forest Meteorology*, 133(1-4): 69-88.
722 Ndehedehe, C.E., Awange, J.L., Corner, R.J., Kuhn, M., Okwuashi, O., 2016. On the potentials of
723 multiple climate variables in assessing the spatio-temporal characteristics of hydrological
724 droughts over the Volta Basin. *Science of the Total Environment*, 557: 819-837.
725 Nijssen, B., Schnur, R., Lettenmaier, D.P., 2001. Global retrospective estimation of soil moisture
726 using the Variable Infiltration Capacity land surface model, 1980-93. *Journal of Climate*,
727 14(8): 1790-1808.
728 Niu, J., 2013. Precipitation in the Pearl River basin, South China: scaling, regional patterns, and
729 influence of large-scale climate anomalies. *Stochastic Environmental Research and Risk*
730 *Assessment*, 27(5): 1253-1268.
731 Niu, J., Chen, J., 2010. Terrestrial hydrological features of the Pearl River basin in South China.
732 *Journal of Hydro-environment Research*, 4(4): 279-288.
733 Niu, J., Chen, J., 2014. Terrestrial hydrological responses to precipitation variability in Southwest
734 China with emphasis on drought. *Hydrological Sciences Journal*, 59(2): 325-335.
735 Niu, J., Chen, J., Sivakumar, B., 2014. Teleconnection analysis of runoff and soil moisture over the
736 Pearl River basin in South China. *Hydrology and Earth System Sciences*, 18(4): 1475-1492.
737 Niu, J., Chen, J., Sun, L.Q., 2015. Exploration of drought evolution using numerical simulations
738 over the Xijiang (West River) basin in South China. *Journal of Hydrology*, 526: 68-77.
739 Niu, J., Chen, J., 2016. A wavelet perspective on variabilities of hydrological processes in
740 conjunction with geomorphic analysis over the Pearl River basin in South China. *Journal of*
741 *Hydrology*, 542: 392-409.

742 Niu, J., Chen, J., Wang, K.Y., Sivakumar, B., 2017. Multi-scale streamflow variability responses to
743 precipitation over the headwater catchments in southern China. *Journal of Hydrology*, 551:
744 14-28.
745 Palmer, W.C., 1965. Meteorological Drought. *U.S. Weather Bureau*, 45: 58.
746 Palmer, W.C., 1968. Keeping track of crop moisture conditions, nationwide: the new crop moisture
747 index. *Weatherwise*, 21: 156-161.
748 Peart, M.R., 2004. Water supply and the development of Hong Kong. *Proceedings of the*
749 *UNESCO/IAHS/IWHA symposium*, 23-30.
750 Pilling, C.G., Jones, J.A.A., 2002. The impact of future climate change on seasonal discharge,
751 hydrological processes and extreme flows in the Upper Wye experimental catchment, mid-
752 Wales. *Hydrological Processes*, 16(6): 1201-1213.
753 PRWRC (Pearl River Water Resources Commission), 2005. Pearl River Flood Prevention
754 Handbook. (in Chinese)
755 Sen, P.K., 1968. Estimates of the regression coefficient based on Kendall's tau. *Journal of the*
756 *American Statistical Association*, 63: 1379-1389.
757 Serinaldi, F., 2016. Can we tell more than we can know? The limits of bivariate drought analyses in
758 the United States. *Stochastic Environmental Research and Risk Assessment*, 30(6): 1691-1704.
759 Shafer, B.A., Dezman, L.E., 1982. Development of a Surface Water Supply Index (SWSI) to assess
760 the severity of drought conditions in snowpack runoff areas. *Proceedings of the Western*
761 *Snow Conference*, 50: 164-175.
762 Shi, H.Y., Wang, G.Q., 2015. Impacts of climate change and hydraulic structures on runoff and
763 sediment discharge in the middle Yellow River. *Hydrological Processes*, 29(14): 3236-
764 3246.

765 Shi, H.Y., Li, T.J., Wei, J.H., Fu, W., Wang, G.Q., 2016a. Spatial and temporal characteristics of
766 precipitation over the Three-River Headwaters region during 1961-2014. *Journal of*
767 *Hydrology: Regional Studies*, 6: 52-65.
768 Shi, H.Y., Li, T.J., Wang, K., Zhang, A., Wang, G.Q., Fu, X.D., 2016b. Physically based
769 simulation of the streamflow decrease caused by sediment-trapping dams in the middle
770 Yellow River. *Hydrological Processes*, 30(5): 783-794.
771 Shi, H.Y., Li, T.J., Wang, G.Q., 2017a. Temporal and spatial variations of potential evaporation
772 and the driving mechanism over Tibet during 1961-2001. *Hydrological Sciences Journal*,
773 62(9): 1469-1482.
774 Shi, H.Y., Li, T.J., Wei, J.H., 2017b. Evaluation of the gridded CRU TS precipitation dataset with
775 the point raingauge records over the Three-River Headwaters region. *Journal of Hydrology*,
776 548: 322-332.
777 Shukla, S., Wood, A.W., 2008. Use of a standardized runoff index for characterizing hydrologic
778 drought. *Geophysical Research Letters*, 35(2): L02405.
779 Sivakumar, M.V.K., Motha, R.P., Wilhite, D.A., Wood, D.A., 2011. Agricultural Drought Indices.
780 *Proceedings of the WMO/UNISDR Expert Group Meeting on Agricultural Drought Indices*,
781 Murcia, Spain.
782 Smirnov, O., Zhang, M.H., Xiao, T.Y., Orbell, J., Lobben, A., Gordon, J., 2016. The relative
783 importance of climate change and population growth for exposure to future extreme
784 droughts. *Climatic Change*, 138(1-2): 41-53.
785 Teegavarapu, R.S.V., 2012. Floods in a Changing Climate: Extreme Precipitation. Cambridge
786 University Press, New York, USA.
787 Thiel, H., 1950. A rank-invariant method of linear and polynomial regression analysis, III.
788 *Proceedings of Koninalijke Nederlandse Akademie van Weinenschatpen*, 53: 1397-1412.

789 Tietjen, B., Schlaepfer, D.R., Bradford, J.B., Lauenroth, W.K., Hall, S.A., Duniway, M.C.,
790 Hochstrasser, T., Jia, G., Munson, S.M., Pyke, D.A., Wilson, S.D., 2017. Climate change-
791 induced vegetation shifts lead to more ecological droughts despite projected rainfall increases
792 in many global temperate drylands. *Global Change Biology*, 23(7): 2743-2754.
793 Trinh, T., Ishida, K., Kavvas, M.L., Ercan, A., Carr, K., 2017. Assessment of 21st century drought
794 conditions at Shasta Dam based on dynamically projected water supply conditions by a
795 regional climate model coupled with a physically-based hydrology model. *Science of the Total*
796 *Environment*, 586: 197-205.
797 United Nations (UN), 1997. Comprehensive Assessment of the Freshwater Resources of the World.
798 http://www.un.org/esa/documents/ecosoc/cn17/1997/ecn171997-9.htm.
799 Vicente-Serrano, S.M., Beguería, S., López-Moreno, J.I., 2010. A multi-scalar drought index
800 sensitive to global warming: the Standardized Precipitation Evapotranspiration Index - SPEI.
801 *Journal of Climate*, 23(7): 1696-1718.
802 Vicuna, S., Gironas, J., Meza, F.J., Cruzat, M.L., Jelinek, M., Bustos, E., Poblete, D., Bambach, N.,
803 2013. Exploring possible connections between hydrological extreme events and climate
804 change in central south Chile. *Hydrological Sciences Journal*, 58(8): 1598-1619.
805 von Storch, H., Navarra, A., 1995. *Analysis of Climate Variability: Applications of Statistical*
806 *Techniques*. Berlin: Springer-Verlag.
807 Wilhite, D.A., Glantz, M.H., 1985. Understanding the drought phenomenon: the role of definitions.
808 *Water international*, 10: 111-120.
809 Wood, A.W., Leung, L.R., Sridhar, V., Lettenmaier, D.P., 2004. Hydrologic implications of
810 dynamical and statistical approaches to downscaling climate model outputs. *Climatic*
811 *Change*, 62: 189-216.

812 Wu, C.H., Xian, Z.Y., Huang, G.R., 2017. Meteorological drought in the Beijiang River basin,
813 South China: current observations and future projections. *Stochastic Environmental*
814 *Research and Risk Assessment*, 30(7): 1821-1834.
815 Wu, H.X., Zhang, Q.T., Zeng, W.H., 2001. Preliminary study of salt water in the Dongjiang delta.
816 *Guangdong Water Resource Hydropower*, 5: 1-3. (in Chinese)
817 Wu, Y.P., Chen, J., 2012. An operation-based scheme for a multiyear and multipurpose reservoir to
818 enhance macroscale hydrologic models. *Journal of Hydrometeorology*, 13(1): 270-283.
819 Wu, Y.P., Chen, J., 2013. Estimating irrigation water demand using an improved method and
820 optimizing reservoir operation for water supply and hydropower generation: A case study of
821 the Xinfengjiang reservoir in southern China. *Agricultural Water Management*, 116: 110-
822 121.
823 Yoo, J., Kim, D., Kim, H., Kim, T.W., 2016. Application of copula functions to construct
824 confidence intervals of bivariate drought frequency curve. *Journal of Hydro-environment*
825 *Research*, 11: 113-122.
826 Zuo, Q.T., 2011. Discussion on the calculation method and threshold of the net-utilization ratio of
827 water resources. *Journal of Hydraulic Engineering*, 42(11): 1372-1378. (in Chinese)
828

Table 1: Definitions of the SEDI based on different levels of water shortage and drought duration.

SEDI		Water shortage level (WSL)		Drought duration level (DDL)	
Value	Definition	Value	Definition	Value	Definition
1	Slight	1	RSP < 40%	1	Quarterly (i.e., 1-3 months)
2	Moderate	2	40% < RSP < 60%	2	Semi-annual (i.e., 4-6 months)
3	Severe	3	60% < RSP < 80%	3	Annual (i.e., 7-12 months)
4	Extreme	4	RSP ≥ 80%	4	More than 12 months

Table 2: Summary of the 52 selected datasets.

Data source (Climate Model)	Emission Scenarios	Horizontal Resolution	Period
16 IPCC AR4 GCMs (1. bccr_bcm2_0.1, 2. ncar_ccsm3_0.1, 3. cccma_cgcm3_1.1, 4. cnrm_cm3.1, 5. csiro_mk3_0.1, 6. mpi_echam5.1, 7. miub_echo_g.1, 8. gfdl_cm2_0.1, 9. gfdl_cm2_1.1, 10. giss_model_e_r.1/2, 11. inmcm3_0.1, 12. ipsl_cm4.1, 13. miroc3_2_medres.1, 14. mri_cgcm2_3_2a.1, 15. ncar_pcm1.1/2, 16. ukmo_hadcm3.1)	SRES A2/A1B/B1	0.5°×0.5°	1951-2099
1 IPCC AR5 GCM (17. HadGEM2-ES)	RCP 2.6/4.5/6.0/8.5	0.5°×0.5°	2000-2099

8 **Table 3**: The slopes (mm/year) of the simulated streamflow at the Boluo station during

9 2020-2099 for each of the 52 datasets. Note: *p* is the significance level.

AR4 scenario	A1B	A2	B1
1. bccr_bcm2_0.1	0.43 (*p*>0.1)	0.11 (*p*>0.1)	1.85 (*p*>0.1)
2. ncar_ccsm3_0.1	2.57 (*p*>0.1)	4.06 (***p*<0.05**)	1.65 (*p*>0.1)
3. cccma_cgcm3_1.1	1.58 (*p*>0.1)	0.03 (*p*>0.1)	0.51 (*p*>0.1)
4. cnrm_cm3.1	2.56 (***p*<0.1**)	2.02 (*p*>0.1)	2.29 (*p*>0.1)
5. csiro_mk3_0.1	-1.72 (*p*>0.1)	-2.33 (*p*>0.1)	0.49 (*p*>0.1)
6. mpi_echam5.1	-2.77 (***p*<0.1**)	0.29 (*p*>0.1)	0.27 (*p*>0.1)
7. miub_echo_g.1	3.38 (***p*<0.05**)	1.51 (*p*>0.1)	1.69 (*p*>0.1)
8. gfdl_cm2_0.1	5.33 (***p*<0.01**)	1.08 (*p*>0.1)	3.89 (***p*<0.05**)
9. gfdl_cm2_1.1	0.44 (*p*>0.1)	3.03 (***p*<0.1**)	4.02 (***p*<0.05**)
10. giss_model_e_r.1/2	3.55 (***p*<0.1**)	4.28 (***p*<0.05**)	1.97 (*p*>0.1)
11. inmcm3_0.1	3.73 (***p*<0.1**)	5.12 (***p*<0.05**)	-0.71 (*p*>0.1)
12. ipsl_cm4.1	-2.22 (*p*>0.1)	2.12 (*p*>0.1)	3.27 (***p*<0.05**)
13. miroc3_2_medres.1	-2.45 (*p*>0.1)	-0.03 (*p*>0.1)	0.25 (*p*>0.1)
14. mri_cgcm2_3_2a.1	3.04 (***p*<0.05**)	2.80 (***p*<0.1**)	5.95 (***p*<0.01**)
15. ncar_pcm1.1/2	2.45 (*p*>0.1)	-0.39 (*p*>0.1)	3.08 (***p*<0.1**)
16. ukmo_hadcm3.1	6.09 (***p*<0.01**)	6.75 (***p*<0.01**)	11.02 (***p*<0.01**)
AR5 scenario	RCP 4.5	RCP 6.0	RCP 8.5
17. HadGEM2-ES	1.24 (*p*>0.1)	2.63 (***p*<0.05**)	3.24 (***p*<0.05**)

10

11

12 **Table 4**: The largest RSP value during 2020-2099 for each of the 52 datasets.

AR4 scenario		A1B	A2	B1
1. bccr_bcm2_0.1		1.48	2.04	1.36
2. ncar_ccsm3_0.1		1.38	2.26	1.83
3. cccma_cgcm3_1.1		1.07	1.64	1.40
4. cnrm_cm3.1		2.85	2.39	1.60
5. csiro_mk3_0.1		3.05	2.22	1.81
6. mpi_echam5.1		1.80	2.26	1.02
7. miub_echo_g.1		0.91	2.07	1.27
8. gfdl_cm2_0.1		1.48	1.93	2.03
9. gfdl_cm2_1.1		1.59	2.05	1.34
10. giss_model_e_r.1/2		1.63	1.39	1.14
11. inmcm3_0.1		1.99	1.99	1.74
12. ipsl_cm4.1		1.17	1.36	1.40
13. miroc3_2_medres.1		1.49	1.99	2.53
14. mri_cgcm2_3_2a.1		1.55	2.00	1.57
15. ncar_pcm1.1/2		1.32	1.72	0.91
16. ukmo_hadcm3.1		1.11	0.94	0.93
Mean of the 16 AR4 GCMs		1.62	1.89	1.49
AR5 scenario	RCP 2.6	RCP 4.5	RCP 6.0	RCP 8.5
17. HadGEM2-ES	0.69	0.77	0.82	0.86

13

14

Table 5: The number of socioeconomic drought events with either longer duration or larger RSP value than the 1963 drought event during 2020-2099 for each of the 52 datasets. Note: the percentages in the parentheses are calculated by dividing the total number of socioeconomic drought events for the corresponding dataset.

AR4 scenario		A1B	A2	B1
1. bccr_bcm2_0.1		29 (28%)	27 (24%)	35 (34%)
2. ncar_ccsm3_0.1		28 (25%)	32 (37%)	32 (30%)
3. cccma_cgcm3_1.1		28 (25%)	30 (28%)	22 (20%)
4. cnrm_cm3.1		38 (45%)	29 (34%)	31 (34%)
5. csiro_mk3_0.1		29 (32%)	34 (37%)	31 (33%)
6. mpi_echam5.1		33 (31%)	35 (36%)	37 (38%)
7. miub_echo_g.1		32 (31%)	33 (31%)	28 (28%)
8. gfdl_cm2_0.1		33 (33%)	31 (32%)	26 (26%)
9. gfdl_cm2_1.1		33 (31%)	32 (34%)	26 (25%)
10. giss_model_e_r.1/2		27 (24%)	18 (15%)	25 (22%)
11. inmcm3_0.1		33 (37%)	39 (45%)	39 (39%)
12. ipsl_cm4.1		31 (32%)	35 (42%)	38 (37%)
13. miroc3_2_medres.1		34 (39%)	33 (32%)	27 (29%)
14. mri_cgcm2_3_2a.1		39 (38%)	36 (40%)	33 (31%)
15. ncar_pcm1.1/2		32 (38%)	31 (31%)	30 (27%)
16. ukmo_hadcm3.1		16 (15%)	19 (16%)	27 (25%)
Mean of the 16 AR4 GCMs		31 (31%)	31 (32%)	30 (30%)
AR5 scenario	RCP 2.6	RCP 4.5	RCP 6.0	RCP 8.5
17. HadGEM2-ES	7 (7%)	7 (7%)	9 (9%)	11 (12%)

Table 6: The numbers of socioeconomic drought events when different percent of the effective storage of the XFJ Reservoir is used under each of the 4 scenarios of the 1 AR5 GCM.

Used percent	RCP 2.6 scenario					RCP 4.5 scenario				
	Total	SEDI =1	SEDI =2	SEDI =3	SEDI =4	Total	SEDI =1	SEDI =2	SEDI =3	SEDI =4
0	97	19	24	53	1	95	16	25	54	0
10%	81	8	37	36	0	80	3	44	33	0
20%	76	16	48	12	0	78	18	51	9	0
30%	69	30	27	2	0	69	36	30	3	0
40%	50	34	16	0	0	53	35	17	1	0
50%	27	24	3	0	0	29	24	5	0	0
60%	8	8	0	0	0	5	4	1	0	0
70%	0	0	0	0	0	3	3	0	0	0
80%	0	0	0	0	0	0	0	0	0	0
90%	0	0	0	0	0	0	0	0	0	0
Used percent	RCP 6.0 scenario					RCP 8.5 scenario				
	Total	SEDI =1	SEDI =2	SEDI =3	SEDI =4	Total	SEDI =1	SEDI =2	SEDI =3	SEDI =4
0	98	21	20	55	2	93	16	27	49	1
10%	79	4	39	35	1	81	9	44	28	0
20%	78	14	53	11	0	76	18	44	14	0
30%	76	33	40	3	0	66	33	27	6	0
40%	61	37	22	0	0	52	37	14	1	0
50%	37	33	4	0	0	22	15	7	0	0
60%	12	12	0	0	0	11	8	3	0	0
70%	2	2	0	0	0	4	4	0	0	0
80%	1	1	0	0	0	1	1	0	0	0
90%	0	0	0	0	0	0	0	0	0	0

Figure

Click here to download Figure: Drought_Figure_R2.doc

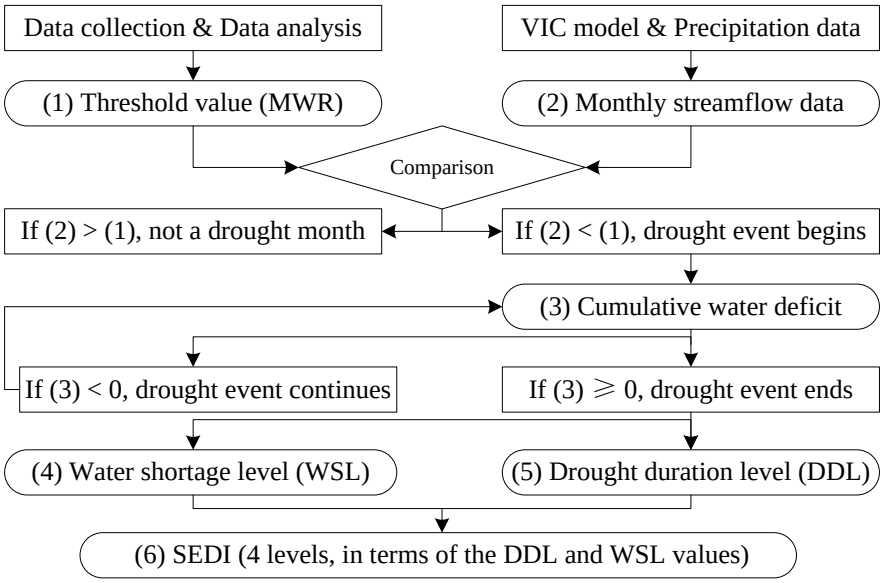

Fig. 1. Flowchart of the development of the heuristic method and the SEDI.

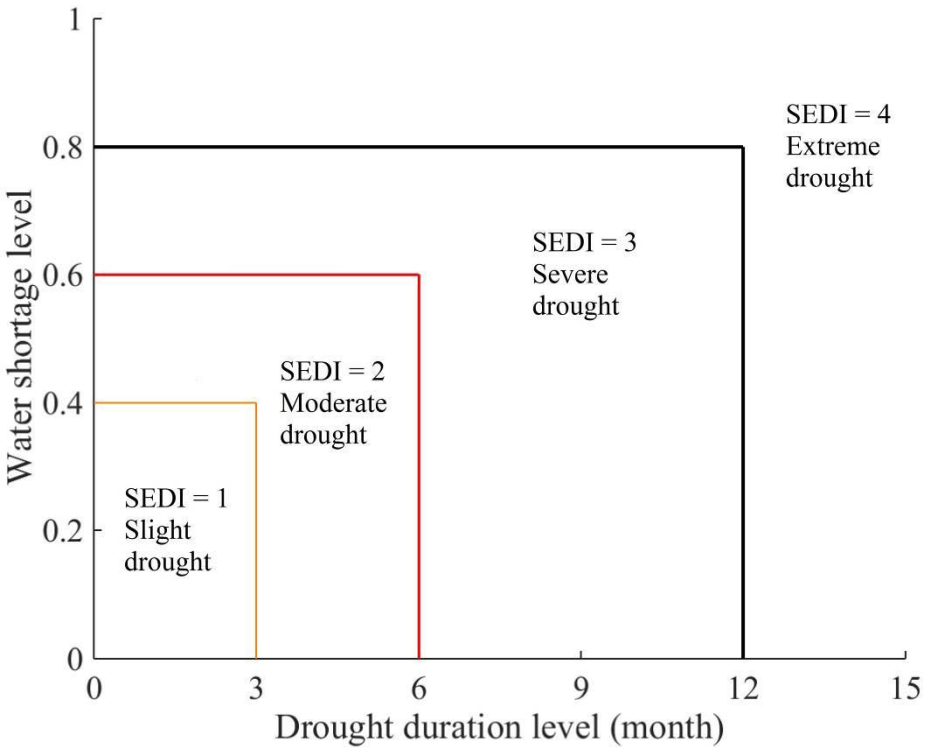

Fig. 2. The ranges of different SEDI values classified by different levels of drought duration and water shortage.

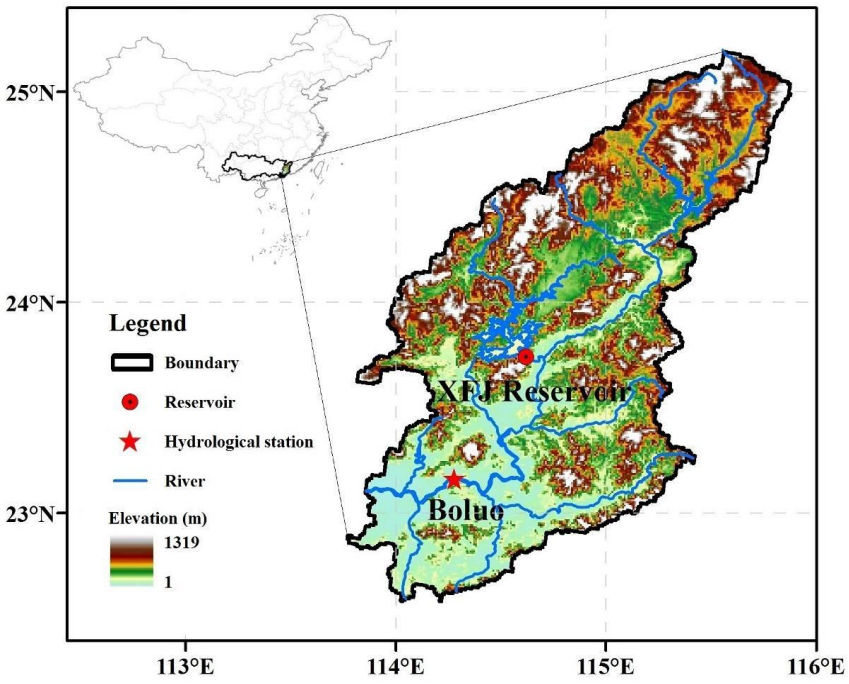

Fig. 3. The Xinfengjiang (XFJ) Reservoir and the Boluo hydrological station in the East River basin.

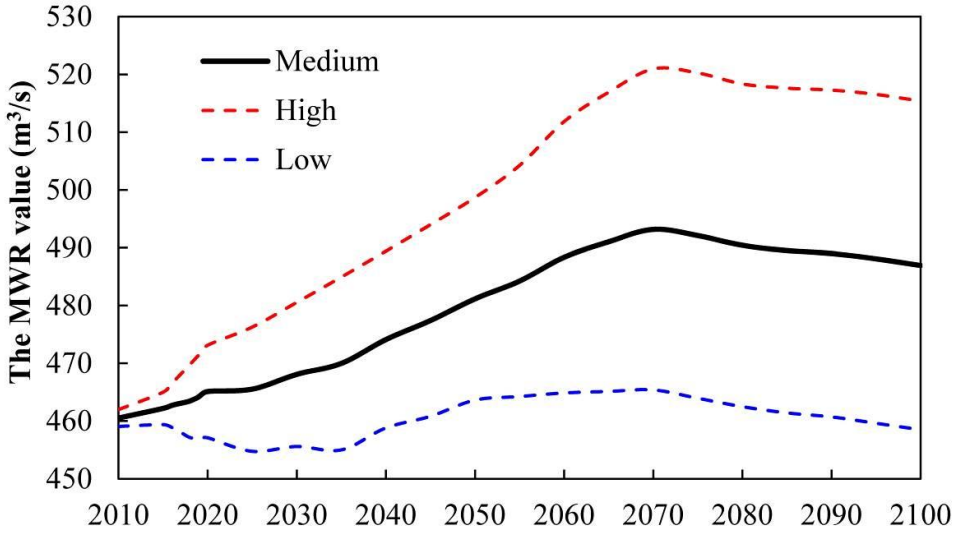

Fig. 4. The MWR value of the East River basin for each year during 2010-2099 under high, medium and low projection scenarios.

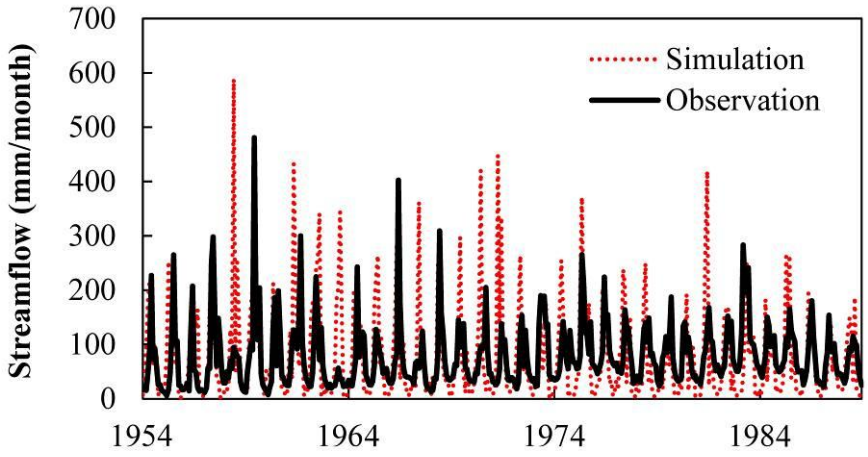

Fig. 5. Comparison of the mean value of the simulated streamflow data from the 48 datasets against the observations for each month during 1954-1988.

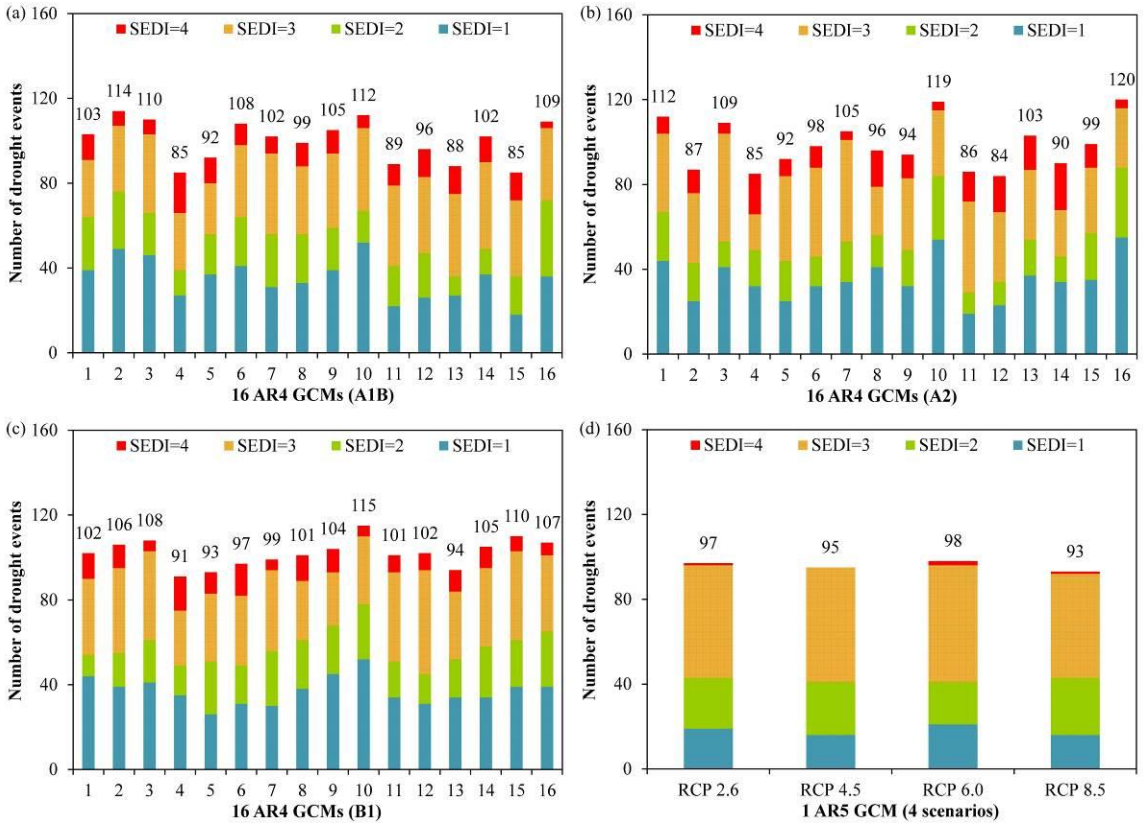

Fig. 6. The numbers of socioeconomic drought events with different SEDI values for each of the 52 datasets (16 AR4 GCMs under the three scenarios and 1 AR5 GCM under the four scenarios).

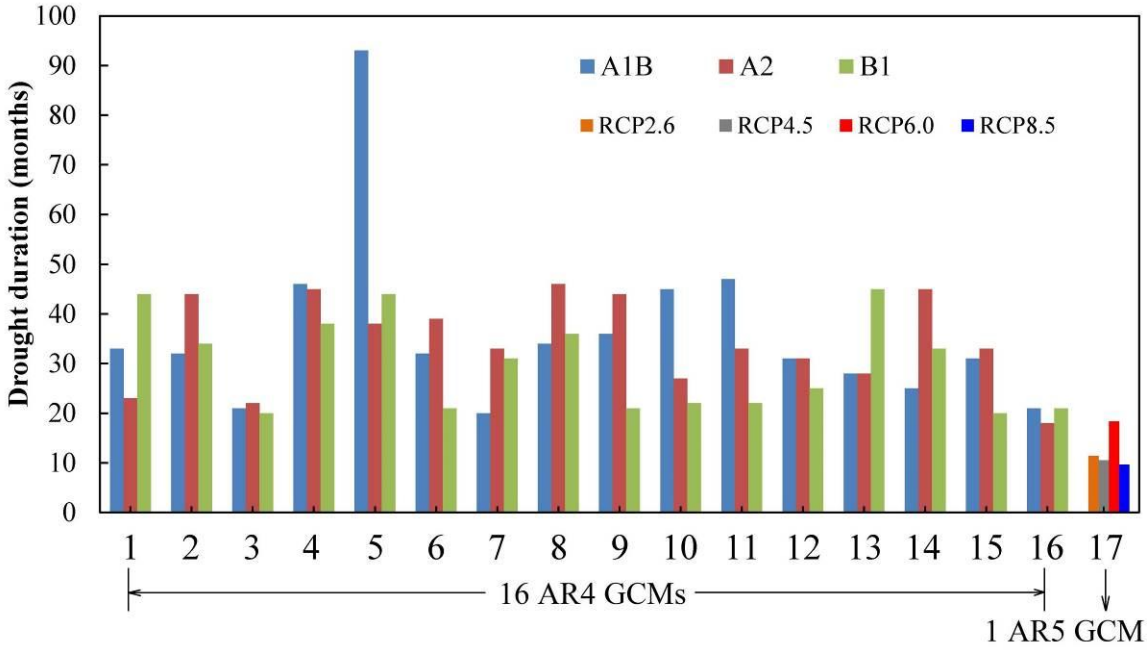

25

26 **Fig. 7.** Socioeconomic drought event with the longest drought duration for each of the 52

27 datasets.

28

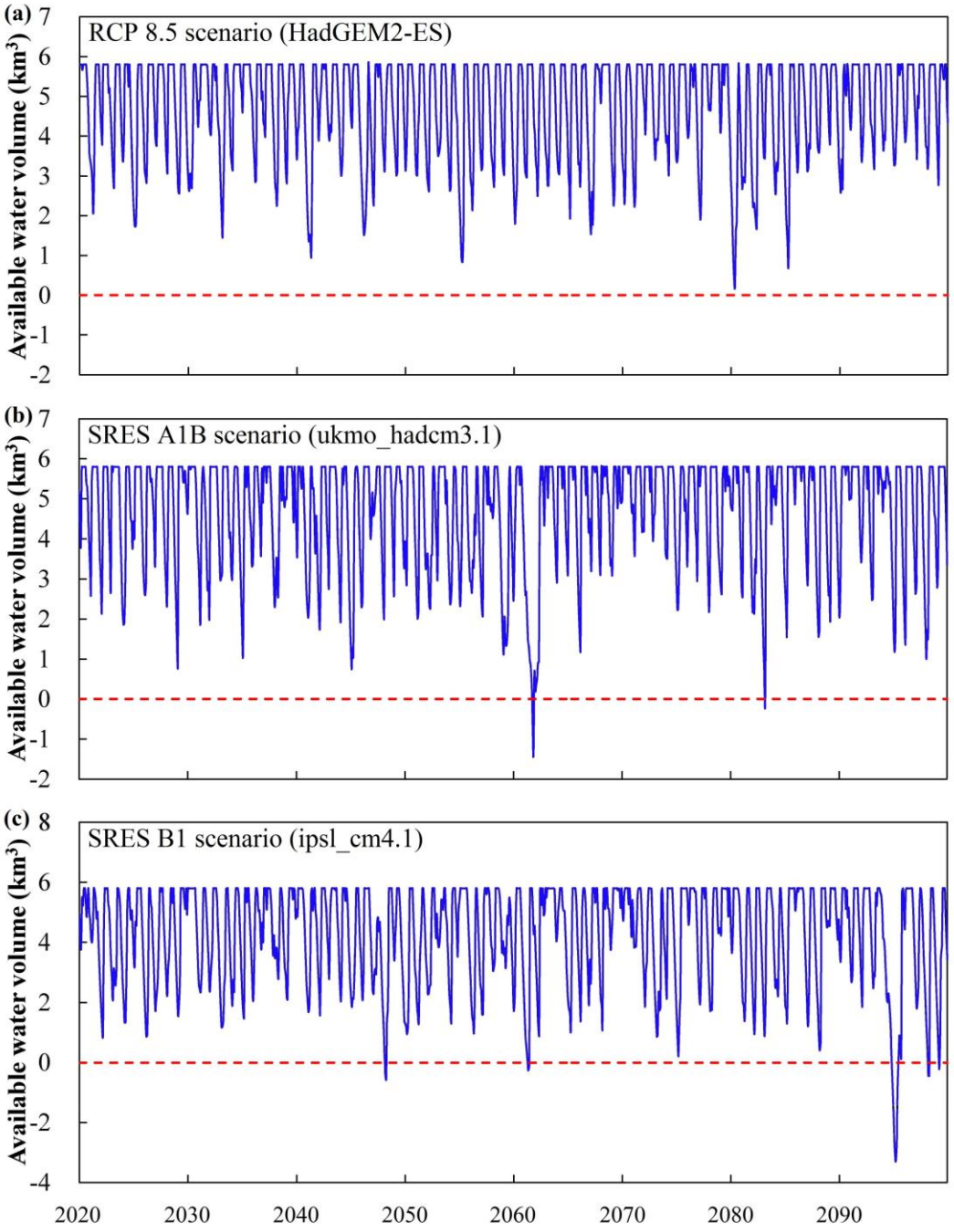

Fig. 8. The monthly available water volume in the XFJ Reservoir during 2020-2099 under three representative scenarios. Note: the red dash lines denote the usable capacity of the XFJ Reservoir (i.e., 5.8 km^3) is run out.

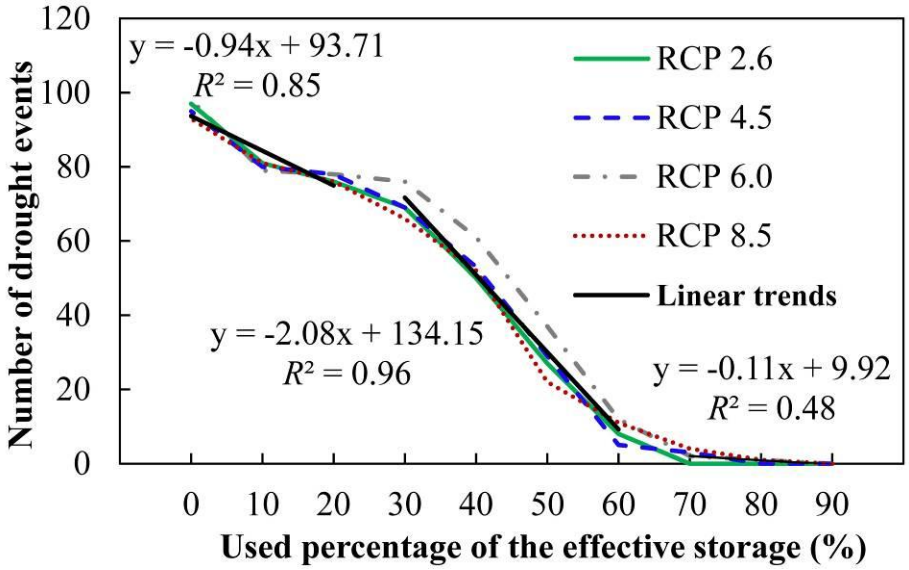

Fig. 9. The relationship between the number of socioeconomic drought events and the used percentage of the effective storage of the XFJ Reservoir based on the 1 AR5 GCM under the four scenarios during 2020-2099. Note: the black lines denote the linear trends.